Dependence of Fast Changes in Global and Local Precipitation on the Geographical Location of Absorbing Aerosol

ANDREW I. L. WILLIAMS,[a] DUNCAN WATSON-PARRIS,[a] GUY DAGAN,[b] AND PHILIP STIER[a]

[a] *Atmospheric, Oceanic and Planetary Physics, Department of Physics, University of Oxford, Oxford, United Kingdom*
[b] *Fredy and Nadine Herrmann Institute of Earth Sciences, Hebrew University of Jerusalem, Jerusalem, Israel*

(Manuscript received 13 January 2023, in final form 3 April 2023, accepted 1 May 2023)

ABSTRACT: Anthropogenic aerosol interacts strongly with incoming solar radiation, perturbing Earth's energy budget and precipitation on both local and global scales. Understanding these changes in precipitation has proven particularly difficult for the case of absorbing aerosol, which absorbs a significant amount of incoming solar radiation and hence acts as a source of localized diabatic heating to the atmosphere. In this work, we use an ensemble of atmosphere-only climate model simulations forced by identical absorbing aerosol perturbations in different geographical locations across the globe to develop a basic physical understanding of how this localized heating impacts the atmosphere and how these changes impact on precipitation both globally and locally. In agreement with previous studies we find that absorbing aerosol causes a decrease in global-mean precipitation, but we also show that even for identical aerosol optical depth perturbations, the global-mean precipitation change varies by over an order of magnitude depending on the location of the aerosol burden. Our experiments also demonstrate that the local precipitation response to absorbing aerosol is opposite in sign between the tropics and the extratropics, as found by previous work. We then show that this contrasting response can be understood in terms of different mechanisms by which the large-scale circulation responds to heating in the extratropics and in the tropics. We provide a simple theory to explain variations in the local precipitation response to absorbing aerosol in the tropics. Our work highlights that the spatial pattern of absorbing aerosol and its interactions with circulation are a key determinant of its overall climate impact and must be taken into account when developing our understanding of aerosol–climate interactions.

KEYWORDS: Atmosphere; Forcing; Precipitation; Radiation; Aerosol optical properties; Biomass burning

1. Introduction

Precipitation is a crucial component of the hydrological cycle and many aspects of human society have evolved in response to the dynamics of regional precipitation (Kathayat et al. 2022). Latent heat release through precipitation is an essential part of the atmospheric energy budget (Pendergrass and Hartmann 2012, 2014; Myhre et al. 2017) and is balanced by changes in atmospheric radiative cooling and sensible heat fluxes on global scales (Allen and Ingram 2002; Myhre et al. 2018). Furthermore, modeling work has suggested a link between the global-mean precipitation response and the equilibrium climate sensitivity (Watanabe et al. 2018). Thus, understanding how human activity is altering the characteristics of precipitation is important from both a scientific and a societal perspective.

Anthropogenic aerosol emissions are known to influence precipitation through a number of pathways. First, increase of aerosol enhances the total atmospheric extinction in a column through scattering and absorption. This reduces the amount of solar radiation reaching the surface and drives a reduction in surface fluxes, which causes global-mean precipitation to decrease due to energy budget constraints (Ramanathan et al. 2001; Samset et al. 2016; Myhre et al. 2017). Additionally, for absorbing aerosol (such as black carbon, dust, or absorbing organic aerosol) the absorption of incident solar radiation heats the atmospheric column and acts as a direct diabatic heating perturbation (Stier et al. 2007; Brown et al. 2021; Williams et al. 2022). This diabatic heating perturbation generally causes a decrease in global-mean precipitation due to energetic constraints (Mitchell et al. 1987; Pendergrass and Hartmann 2014). Anthropogenic aerosol can also influence precipitation on regional scales by influencing the microphysical properties of clouds (Albrecht 1989; Levin and Brenguier 2009; Dagan et al. 2017; Herbert et al. 2021), although this pathway is subject to considerable uncertainty (Stevens and Feingold 2009; Seifert et al. 2015), and thus, in our current work we focus purely on the precipitation changes arising from aerosol–radiation interactions (ARI).

The response of precipitation to anthropogenic aerosol is commonly decomposed into "fast" and "slow" contributions (Samset et al. 2016; Voigt et al. 2017; Zhang et al. 2021). Fast responses, also referred to as rapid adjustments, occur in the

Denotes content that is immediately available upon publication as open access.

Supplemental information related to this paper is available at the Journals Online website: https://doi.org/10.1175/JCLI-D-23-0022.s1.

Williams's current affiliation: Princeton Program in Atmosphere and Ocean Sciences, Princeton University, Princeton, New Jersey.
Watson-Parris's current affiliation: Scripps Institution of Oceanography, and Halicioğlu Data Science Institute, University of California, San Diego, La Jolla, California.

Corresponding author: Andrew I. L. Williams, andrew.williams@noaa.gov

DOI: 10.1175/JCLI-D-23-0022.1

first hours or weeks following the perturbation (Stjern et al. 2023) and are independent of sea surface temperature (SST) changes (and so are efficiently studied using fixed-SST simulations). Slow responses occur in the years and decades following the perturbation and are mediated by the SST changes. Some examples of the slow contribution to precipitation changes would be shifts of the intertropical convergence zone (ITCZ) (Wang 2004, 2007, 2015; Ming and Ramaswamy 2009, 2011; Voigt et al. 2017; Zhang et al. 2021) or changes in monsoon precipitation (Tian et al. 2018; Dong et al. 2016, 2019; Xie et al. 2020).

For the case of absorbing aerosol (such as black carbon), the Precipitation Driver Response Model Intercomparison Project (PDRMIP) (Myhre et al. 2017) has shown that the fast response dominates the global-mean precipitation response, and that this is unique among the forcers they studied (Samset et al. 2016; Stjern et al. 2017). Furthermore, the intermodel spread in fast precipitation responses to absorbing aerosol are dominated by aerosol-driven rapid adjustments in clouds and circulation. Rapid adjustments are particularly complicated for absorbing aerosol due to the fact that through absorption of incoming solar radiation, the aerosol acts as a source of diabatic heating to the atmospheric column (Johnson et al. 2019; Williams et al. 2022). This localized diabatic heating can have significant impacts on the atmospheric thermodynamics and circulation by influencing moist processes, particularly in the tropics where clouds and circulation are intricately linked through radiative transfer, phase changes and SSTs.

In summary, the response of precipitation to absorbing aerosol perturbations is still uncertain and a significant portion of this uncertainty can be attributed to difficulties in understanding the "fast" response of clouds and circulation to the localized diabatic heating which results from aerosol absorption of solar radiation. Much of the previous work on this question has used either emissions-driven simulations (e.g., Westervelt et al. 2018; Persad and Caldeira 2018), which are more realistic but bring with them the uncertainties associated with the conversion of aerosol emissions to aerosol concentrations, or concentration-driven simulations (e.g., Samset et al. 2016), which require a further region-dependent mapping from aerosol concentrations to absorptivity. Taken together, this has made it difficult to explore the fundamental mechanisms which control the atmospheric response to regional aerosol heating.

Furthermore, previous studies have often focused on perturbations in a small number of regions. This is a sensible trade-off given the added complexity of emission-driven simulations (Persad and Caldeira 2018) or the desire to have multiple models to compare between (Myhre et al. 2017), but does make it harder to understand the generality of these results, particularly because absorbing aerosol has a highly inhomogeneous spatial distribution (Kinne et al. 2013).

Recently, there has been work using aquaplanet (Dagan et al. 2019) and AMIP-style (Dagan et al. 2021) simulations with prescribed aerosol radiative properties to understand the influence of aerosol–radiation interactions on precipitation—which circumvents the translation from emissions to concentrations to absorption mentioned above. Interestingly, this work has shown that the local precipitation response to absorbing aerosol is positive in the tropics and negative in the extratropics, and has explained these responses using the local atmospheric energy budget. However, although these results are qualitatively similar between the aquaplanet simulations and AMIP-style simulations with land, only a few locations have been tested in AMIP-style simulations, and thus, it is unclear how the location of the aerosol perturbation mediates these changes.

To tackle these questions, we have used a large set of atmosphere-only simulations forced by identical absorbing aerosol perturbations across the whole globe to explore the sensitivity of the global- and local-precipitation response to absorbing aerosol. Our idealized experimental setup also allows us to better understand the physical mechanisms involved compared to previous work (Persad and Caldeira 2018; Samset et al. 2016; Persad 2023), and thus, we are able to explicitly link the precipitation responses to the fundamental physics governing the atmospheric circulation response to diabatic heating in different regions.

2. Methods

a. *Experiment design*

The experiments conducted in this study adopted the same design of Williams et al. (2022) to investigate the sensitivity of effective radiative forcing to changes in the spatial pattern of absorbing aerosol, and more details can be found there.

An ensemble of 145 fixed-SST simulations were conducted using the Icosahedral Nonhydrostatic (ICON) general circulation model (icon-aes-1.3.00), which has a newly developed dynamical core and has been tuned to give a well-balanced top-of-atmosphere radiation budget and reasonable representation of precipitation compared to other atmosphere-only models and to observations (Crueger et al. 2018; Giorgetta et al. 2018). The model uses a bulk mass-flux convection scheme (Tiedtke 1989; Nordeng 1994), with cloud cover calculated locally using a relative humidity scheme (Sundqvist et al. 1989). Cloud microphysics is based on the Lohmann and Roeckner scheme (Lohmann and Roeckner 1996); however, the droplet number is fixed to prescribed profiles over land and ocean (Stevens et al. 2013) and the model does not simulate aerosol–cloud interactions. Radiation is parameterized using the PSrad radiative transfer scheme (Pincus and Stevens 2013). The radiation scheme is called two times (both all sky and clear sky) at every radiation time step, once with aerosol and once without aerosol. Taking the difference between these two "double calls" gives the total aerosol radiative effect, and the instantaneous aerosol radiative forcing is calculated by differencing the total aerosol radiative effect between a perturbed run and the control.

The simulations were run on a triangular grid (R_2B_4 specification) corresponding to an approximately uniform horizontal grid spacing of 160 km. The model uses a terrain-following vertical sigma-height grid (Leuenberger et al. 2010) with 47 levels between the surface and the model top at 83 km. Each simulation, including the control run, is integrated for 20 years, after which the first year is discarded as spinup and

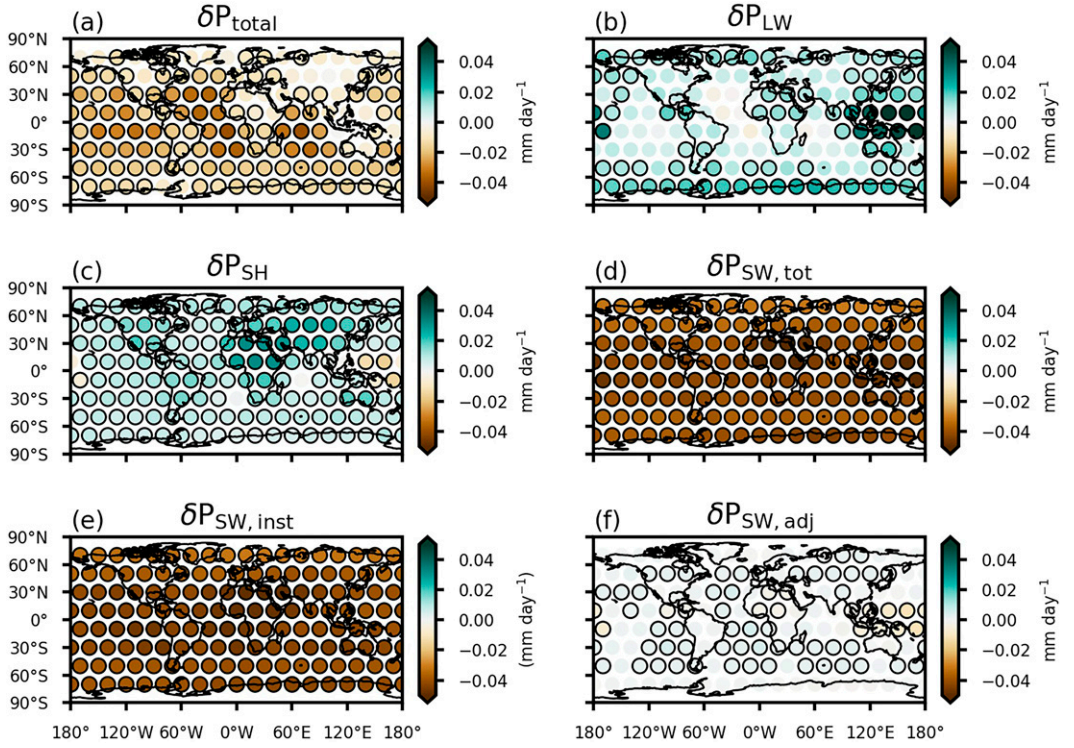

FIG. 1. (a) Global- and time-mean changes in precipitation and (b) contributions from changes in longwave cooling, (c) surface sensible heat flux, and (d) shortwave absorption according to Eq. (2). (e),(f) A further decomposition of the shortwave absorption term into contributions from instantaneous radiative fluxes and rapid adjustments, respectively. Each colored circle represents the results from the simulation imposing an aerosol perturbation in that location. Black enclosing circles are present where the time series of global- and annual-mean changes are statistically different from zero at the 99% level according to a one-sided *t* test.

analysis is conducted over the remaining 19 years. The simulation length was chosen as a trade-off between computational constraints and the requirement that our runs are long enough to give robust results in the face of internal variability.

As we are focusing on the "fast" response of precipitation to anthropogenic absorbing aerosol, we run the simulations with a prescribed monthly climatology of sea surface temperatures and sea ice concentrations derived from time-averaged Atmospheric Model Intercomparison Project (AMIP) (Gates 1992) boundary conditions over the 1979–2016 period.

Aside from the control run, the only difference between the remaining 144 simulations is the inclusion of an idealized plume of absorbing aerosol at 144 different geographical locations (Fig. 1a), parameterized using the Max Planck Institute Aerosol Climatology, version 2, Simple Plume (MACv2-SP) model (Stevens et al. 2017). The extinction is prescribed at 550 nm and then extrapolated to other wavelengths in the shortwave spectrum using an Ångström parameter of 2; no aerosol extinction is prescribed in the longwave. The plume's horizontal structure is specified to be a two-dimensional Gaussian function with a standard deviation of 10°. The vertical distribution of aerosol is based on the kernel of Euler's β function (see details in Stevens et al. 2017), with most of the aerosol concentrated in the lower 3 km of the atmosphere and a peak at ≈1 km (online supplementary Fig. 1). We note that differences in the vertical plume profile may cause different responses of the climate system and general circulation (Persad et al. 2012; Ban-Weiss et al. 2012); however, Williams et al. (2022) showed that their results were robust to realistic variations in the shape and height of the aerosol perturbation. Both the horizontal and vertical structure of the plume are constant in time and the shape of the plume is not influenced by the local meteorology.

In each of the aerosol perturbation experiments the plume is prescribed with a total column AOD = 1 and a single-scattering albedo (SSA) of 0.8, both defined at a wavelength of 550 nm. This corresponds to a strongly absorbing plume of aerosol, generating a large diabatic heating perturbation in the lower atmosphere, even while generating cooling at the surface (primarily over land in our experiments due to the use of fixed SSTs). Furthermore, to isolate the role of the radiative impact of the plume we do not include the microphysical effects of the aerosol plume which are also described in Stevens et al. (2017).

b. Atmospheric energy budget decomposition

From an energetic perspective, on global scales and at equilibrium, the net energy input to the atmosphere (shortwave absorption of incoming solar radiation and latent heat released by precipitation) must be balanced by atmospheric radiative cooling and surface sensible heat fluxes (Muller and O'Gorman 2011;

Pendergrass and Hartmann 2014; Dagan et al. 2021; Zhang et al. 2021). Mathematically we can write this as

$$LP + Q_{SW} = Q_{LW} + SH, \quad (1)$$

where L is the latent heat of condensation of water vapor, P is the precipitation rate, Q_{SW} is the shortwave absorption, Q_{LW} is the longwave radiative cooling, and SH is the upward sensible heat flux at the surface. Taking a difference between our control simulation and simulations with an absorbing aerosol perturbation and rearranging yields a well-known constraint on the global-mean precipitation change associated with an anthropogenic perturbation (e.g., Myhre et al. 2018; Allen and Ingram 2002):

$$L\delta P = \delta Q_{LW} - \delta Q_{SW} + \delta SH. \quad (2)$$

We use Eq. (2) to understand the fast changes (i.e., under fixed SSTs) in global-mean precipitation in each of our 144 absorbing aerosol experiments. We calculate the Q_{LW} and Q_{SW} terms in Eq. (2) as follows:

$$Q_{LW} = LW^{\uparrow}_{TOA} + (LW^{\downarrow}_{SFC} - LW^{\uparrow}_{SFC}) \quad \text{and} \quad (3)$$

$$Q_{SW} = (SW^{\downarrow}_{TOA} - SW^{\uparrow}_{TOA}) + (SW^{\uparrow}_{SFC} - SW^{\downarrow}_{SFC}), \quad (4)$$

with all fluxes defined as positive upward. We further decompose the δQ_{SW} into a component associated with the *instantaneous* change in radiative fluxes associated with the inclusion of the aerosol, δQ^{inst}_{SW}, and a component that represents the change in Q_{SW}, δQ^{adj}_{SW}, which results from rapid adjustments, such as changes in clouds, atmospheric water vapor or surface albedo.

All of the terms on the right-hand side of Eq. (2) are initially calculated in energy units (W m^{-2}), before being transformed into "precipitation units" (mm day^{-1}) for ease of presentation.

3. Sensitivity of global-mean precipitation to localized absorbing aerosol perturbations

In Fig. 1 we have plotted the change in global-mean precipitation associated with each of the 144 absorbing aerosol experiments conducted (Fig. 1a), along with a decomposition [following Eq. (2)] into contributions from longwave cooling (Fig. 1b), surface sensible heat fluxes (Fig. 1c), and shortwave absorption (Fig. 1d). Figures 1e and 1f decompose the changes in shortwave absorption into changes arising from instantaneous changes and rapid adjustments, respectively. Furthermore, to aid interpretation, changes in shortwave absorption have been multiplied by −1 in Figs. 1d–f [to account for the negative sign in Eq. (2)] so that the total precipitation change in Fig. 1a can be reconstructed by summing Fig. 1b + Fig. 1c + Fig. 1d.

There is a remarkable amount of variation in the global-mean precipitation change in response to the absorbing aerosol plumes in different locations (Fig. 1a). This is particularly striking as the aerosol perturbation in each of these experiments is identical and only the location is varied. All aerosol locations result in a decrease in global-mean precipitation, but the response is weaker over parts of Northern Hemisphere land, and the Sahara. Notably, the response of global-mean precipitation to absorbing aerosol over the western tropical Pacific is also negligible.

a. Contribution from shortwave absorption

To first order, the decrease in global-mean precipitation is set by the additional shortwave absorption of incoming solar radiation (δP_{SW}, Fig. 1d), which results from the inclusion of the absorbing aerosol plumes. Most of this change is due to the contribution from instantaneous radiative fluxes, as shown in Fig. 1e. This contribution drops off slightly toward higher latitudes due to reductions in incoming solar radiation (supplementary Fig. 2). Rapid adjustments also contribute toward changes in shortwave absorption, but this is a much smaller effect (Fig. 1f), and occurs primarily in response to absorbing aerosol over the western tropical Pacific, which is associated with a strong convective response to diabatic heating as demonstrated by Williams et al. (2022). Overall, the contribution of δP_{SW} to global-mean precipitation changes is rather agnostic to the longitudinal position of the absorbing aerosol plume.

b. Contribution from sensible heat fluxes

The sensitivity of fast changes in global-mean precipitation to variations in the geographical position of absorbing aerosol arises predominantly through changes in SH flux and longwave cooling and (Figs. 1c,b, respectively). First, we focus on the SH contribution. The SH flux contributes positively to the global-mean precipitation change for almost all locations, indicating a reduction in the global-mean upward surface sensible heat flux. This positive contribution offsets some of the negative global-mean precipitation changes associated with increased shortwave absorption (particularly over land). The reduction in global-mean upward sensible heat flux (and thus positive contribution to global-mean precipitation changes) occurs because lofted aerosol tends to generate local surface cooling due to the reduction in incoming solar radiation from absorption and scattering processes (e.g., Muller and O'Gorman 2011; Samset et al. 2016; Dagan et al. 2020; Williams et al. 2022). The particularly strong reduction in SH fluxes in response to absorbing aerosol over the Sahara and the Eurasian continent is associated with stronger local surface cooling over this region in response to the plume, and contributes to a muted response of global-mean precipitation in response to absorbing aerosol over these regions.

The exception to this occurs in response to absorbing aerosol over the western tropical Pacific, where the SH changes contribute negatively to global-mean precipitation, which indicates an increase in global-mean upward surface sensible heat flux in response to absorbing aerosol in these regions. This can be understood by noting that absorbing aerosol over this region is associated with a strong convective response, an increase in upper-level divergence and a strengthening of the tropical Walker circulation (as shown previously by Williams et al. 2022). This strengthening of the Walker circulation is associated with an intensification of low-level winds, which increases the upward surface sensible heat flux. It should be noted that black carbon has been found to also increase the lower tropospheric stability and thus reduce surface SH fluxes

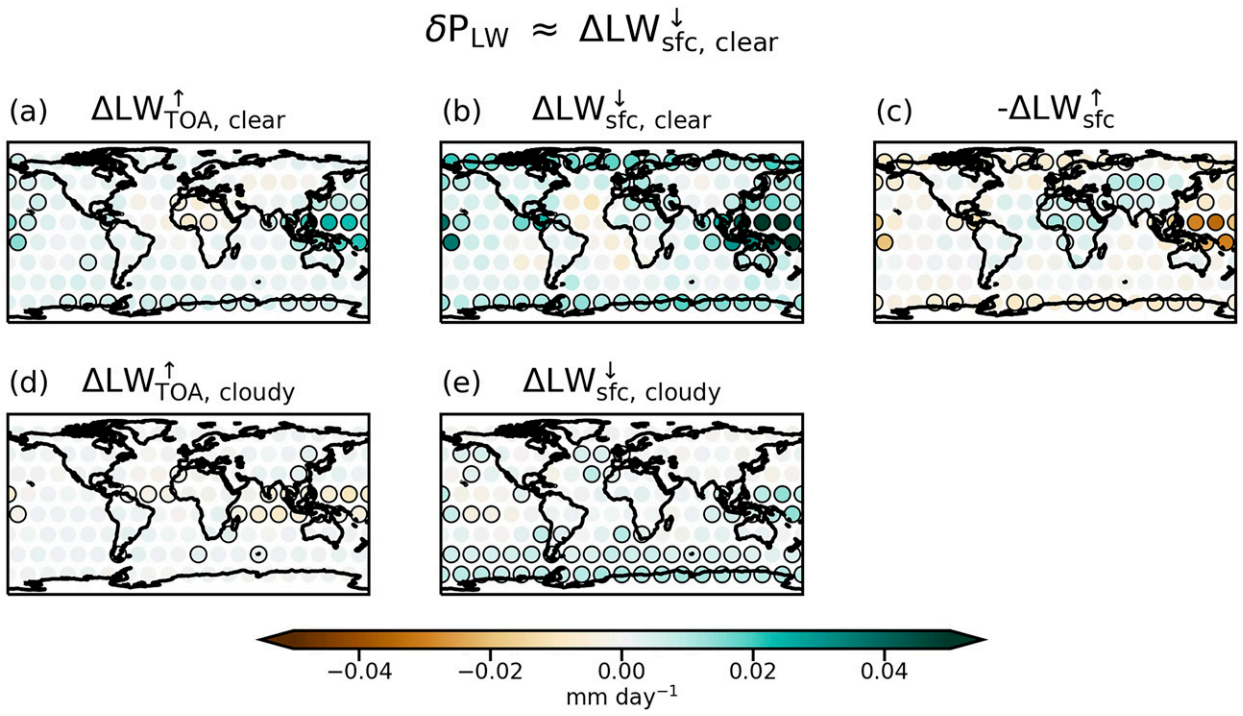

FIG. 2. Decomposition of δP_{LW} into contributions from changes in outgoing LW radiation at top-of-atmosphere in (a) clear and (d) cloudy sky, downward LW emission at the surface in (b) clear and (e) cloudy sky, and (c) upward LW emission at the surface. Each colored circle represents the results from the simulation imposing an aerosol perturbation in that location.

(Myhre et al. 2018), but in our experiments the dominant mechanism appears to be an intensification of the large-scale tropical circulation and low-level winds.

c. *Contribution from longwave cooling*

In addition to sensible heat flux, changes in global-mean atmospheric longwave cooling are also a large contributor to the "location dependence" of fast changes in global-mean precipitation (δP_{LW}, Fig. 1b). Generally, δP_{LW} contributes positively to changes in global-mean precipitation, and there is a notable "hotspot" of positive δP_{LW} in response to absorbing aerosol over the western tropical Pacific (Fig. 1b). In our experiments, changes in global-mean longwave cooling are dominated by changes in clear sky rather than cloudy sky (Fig. 2). To a good approximation, the global-mean changes in longwave cooling are largely controlled by changes in downwelling longwave emission from the atmosphere to the surface (cf. Figs. 1b and 2b). We also note that there is a negative contribution from cloudy-sky outgoing LW radiation, which is consistent with the strong convective response over this region generating more anvil clouds which reduce the outgoing LW radiation locally.

To gain some intuition for what controls these changes in $LW^{\downarrow}_{sfc,clear}$, we assume that they arise due to changes in lower-tropospheric temperature and associated changes in blackbody emission. If we assume that the emission from the lower troposphere can be approximated as σT^4_{850}, then the predicted change in $LW^{\downarrow}_{sfc,clear}$ following a change in global-mean 850-hPa temperature (ΔT_{850}) is equal to $4\sigma T^3_{850}\Delta T_{850}$. In Fig. 3 we show that this estimate captures most of the variation in global-mean clear-sky, downwelling LW emission across our plume experiments, and in particular the large values of $\Delta LW^{\downarrow}_{sfc,clear}$, which occur in response to absorbing aerosol over the western tropical Pacific. The results in Fig. 3 are not sensitive to the precise vertical level we choose. We note that our "temperature-only" scaling of $LW^{\downarrow}_{sfc,clear}$ generally underestimates the true response, and this is likely because it does not include the effect of

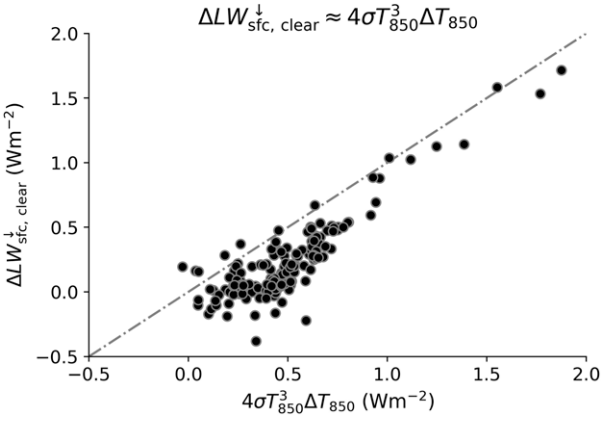

FIG. 3. Scatterplot of global-mean changes in clear-sky, downwelling LW emission from the atmosphere to the surface vs an estimate of these changes, which accounts only for altered blackbody emission from the 850-hPa layer.

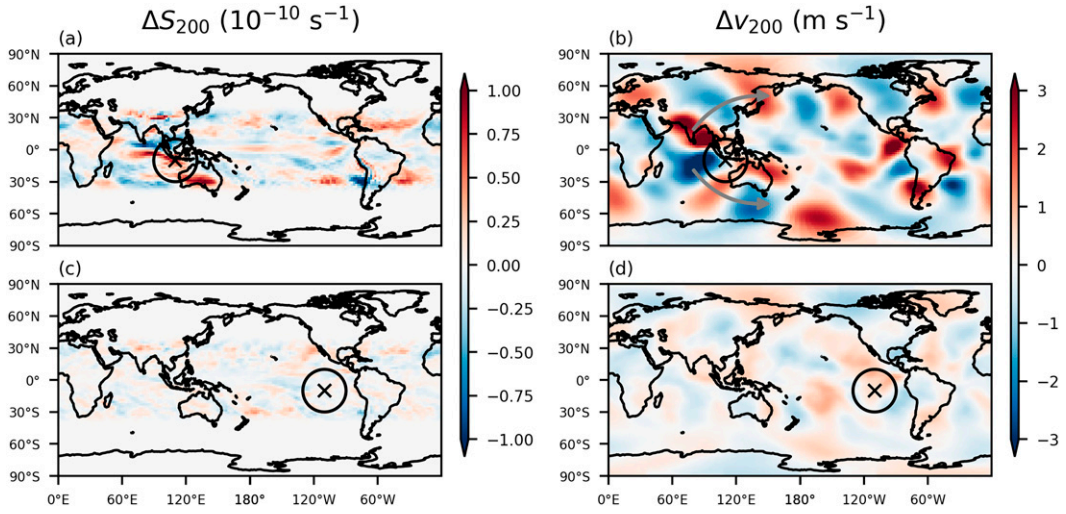

FIG. 4. The change in 200-hPa Rossby wave source (ΔS_{200}) for absorbing aerosol in (a) the western tropical Pacific and (c) the eastern tropical Pacific. To focus on the tropical component of the Rossby wave source, the fields have been linearly tapered to zero between 30° and 40° of the equator. The change in 200-hPa meridional wind (Δv_{200}) for absorbing aerosol in the (b) western tropical Pacific and (d) the eastern tropical Pacific. A stationary Rossby wave train (highlighted by the gray arrows) that emanates from the Indian Ocean into the midlatitudes in both hemispheres can be seen in (b), whereas no such change occurs in response to the absorbing aerosol in the eastern tropical Pacific in (d).

increases in water vapor in response to the aerosol plume, which would also increase $\Delta LW^{\downarrow}_{sfc,clear}$.

We have now shown that changes in clear-sky downwelling LW emission are the dominant contributor to δP_{LW} (Fig. 2), and generally contribute to an increase in global-mean precipitation, with a hotspot of positive global-mean δP_{LW} in response to absorbing aerosol over the western tropical Pacific (Fig. 1b). We have also shown that these changes in downwelling LW emission are highly correlated with changes in tropospheric temperatures (Fig. 3). So, the question now becomes: Why does absorbing aerosol generally increase tropospheric temperatures, and cause such a large increase when placed in the western tropical Pacific?

As we discussed earlier, absorbing aerosol warms the atmosphere locally through absorbing incoming solar radiation. This explains why the changes in Fig. 2b are generally positive, as the absorption warms the atmosphere aloft and causes and increase in downwelling LW emission. With regards to the hotspot of strong δP_{LW} over the western tropical Pacific, this arises primarily because the western tropical Pacific is a region of intense and persistent deep convection throughout the annual cycle. One of the cornerstones of our understanding of tropical dynamics, the "convective quasi-equilibrium" hypothesis, states that deep convection acts to maintain a moist adiabatic temperature profile which is pegged to the temperature of the lower troposphere (e.g., Emanuel 2007). Hence, when absorbing aerosol is placed in the western tropical Pacific, it is able to warm the whole atmospheric column due to the action of deep convection. This warming of the local atmospheric column is then transmitted horizontally across the whole of the tropical free troposphere through the action of gravity waves (Sobel et al. 2001). As a result, absorbing aerosol in the western tropical Pacific is able to cause strong, nonlocal warming of the whole tropical free troposphere. This mechanism appears to be less efficient in other regions of the tropics which are typically associated with deep convection (e.g., the Amazon). This is potentially because the interactive land surface enables surface cooling from the aerosol scattering and absorption to take hold and reduce the subcloud buoyancy (we will discuss this point in more detail in section 4).

While tropical warming contributes to increased δP_{LW} in response to absorbing aerosol over the western tropical Pacific, the hotspot of δP_{LW} over the western tropical Pacific (Fig. 1b) also has an additional, smaller contribution from the extratropics (supplementary Fig. 3). This raises the question: How can an absorbing aerosol perturbation in the tropics influence the extratropics? A potential explanation for this is that absorbing aerosol plumes over this region are associated with a strong convective response and an increase in upper-level divergence (Williams et al. 2022). Previous work (e.g., Sardeshmukh and Hoskins 1988) has shown that tropical upper-level divergence is associated with teleconnections to the midlatitudes because the upper-level divergence can act as a vorticity source, and the resultant Rossby waves then propagate along great-circle paths into the midlatitudes. Figure 4b shows the response of 200-hPa meridional wind to absorbing aerosol in the western tropical Pacific, and a stationary Rossby wave can be seen to propagate from the tropics into the extratropics. In contrast, absorbing aerosol in the east Pacific is not associated with such a teleconnection (Fig. 4d). The plume in Fig. 4b was chosen because it most clearly demonstrates the Rossby wave train, but wave trains exist for most of the western tropical Pacific plumes.

To better quantify this proposed teleconnection mechanism, in Figs. 4a and 4c we plot the Rossby wave source (S) calculated following Sardeshmukh and Hoskins (1988) as

$$S = -\mathbf{u}_\chi \cdot \nabla(\zeta + f) - (\zeta + f)\nabla \cdot \mathbf{u}_\chi, \tag{5}$$

where $\mathbf{u}_\chi$ is the divergent component of the horizontal wind, ζ is the relative vorticity, and f is the planetary vorticity; all terms are taken at 200 hPa. In simple terms, Eq. (5) has two contributions. The first term represents vorticity advection by the divergent wind, meanwhile the second term represents the generation of vorticity by "vortex stretching." This "vortex stretching" term arises as a consequence of angular momentum conservation. For example, upper-level divergence (like that generated by deep convection) means $\nabla \cdot \mathbf{u}_\chi > 0$, which causes the fluid column to elongate and contract. This contraction causes a spinup (increase in vorticity) in the same way as an ice skater spins up when they "contract."

Figures 4a and 4c show the change in 200-hPa Rossby wave source (ΔS_{200}) for absorbing aerosol in the western and eastern tropical Pacific, respectively. To focus on the tropical wave source (which is more relevant for our mechanism) we have tapered the ΔS_{200} fields to zero between 30° and 40° of the equator. Figure 4a demonstrates that the western Pacific aerosol generates a significant Rossby wave source to the west of the perturbation, with a positive ΔS_{200} south of the equator and a negative ΔS_{200} north of the equator. This region of strong ΔS_{200} also corresponds to the region of initiation of the stationary Rossby wave in Fig. 4b, which begins in the Indian Ocean, westward of the absorbing aerosol itself. In contrast, the ΔS_{200} perturbation is negligible for the aerosol perturbation in the east Pacific.

Having propagated across the Pacific basin, the Rossby wave train becomes less pronounced (Fig. 4b), and this is likely due to the twin influences of orography and interference with additional Rossby waves which are initiated in response to the Rossby wave source hotspots in the tropical Atlantic and eastern Pacific (Fig. 4a). It is also worth noting that while upper-level divergence in the tropics can act as a Rossby wave source, whether or not the Rossby waves can propagate into the midlatitudes depends sensitively on the background zonal winds, which can act as atmospheric "waveguides" which determine the turning latitude of the waves (Hoskins and Ambrizzi 1993). As a result, the ability of the Rossby waves to propagate into the midlatitudes depends not only on the upper-level divergence but also the local state of the upper-level zonal winds. This, along with a reduced convective response over land in response to the aerosol (which we will discuss further in section 4), helps explain why we do not see strong Rossby wave responses in other parts of the tropics.

To summarize this section, we have shown that global-mean changes in surface sensible heat fluxes and longwave atmospheric cooling are a strong determinant of the "location dependence" of fast, global-mean precipitation changes in response to absorbing aerosol in different locations. The sensible heat flux changes are most important over land and over regions where the surface cooling from aerosol absorption and scattering is most pronounced (viz., the Sahara and Eurasia). The longwave cooling term also contributes to this location dependence, and these changes are controlled to first order by downwelling emission from the atmosphere to the surface. We have argued that these changes can be explained largely by changes in lower-tropospheric temperatures, which explains the general positive contribution of this term to the global-mean precipitation changes as absorbing aerosol tends to warm the atmosphere aloft. We also noted a hotspot of δP_{LW} in response to absorbing aerosol over the western tropical Pacific, which are associated with global-scale changes in temperature and downwelling LW emission. To explain this, we argue that the western tropical Pacific is unique in two regards. First, heating in this region is able to be communicated across the entire tropical free troposphere due to persistent deep convection, which transports energy in the vertical, and the action of gravity waves which efficiently homogenize temperatures in the tropical free troposphere. Second, heating in the western tropical Pacific also has the potential to influence the extratropics through generating upper-level divergence and exciting a Rossby wave train. The precise mechanisms by which these Rossby wave trains influence the extratropics are difficult to disentangle in our experiments, in part because we only archived monthly mean data. However, one plausible explanation could be that the Rossby waves generate an increase in the poleward eddy heat flux (Chemke and Polvani 2020), thus transferring more heat from the tropics to the extratropics. Another possible explanation could involve the fact that Rossby waves generally induce an alternating pattern anomalous poleward and equatorward flow (as can be seen in Fig. 4b). If the regions of anomalous poleward flow coincide with land regions (which have interactive surface temperatures) but the regions anomalous equatorward flow coincide most with ocean regions (with fixed SSTs) then this could also generate an increase in extratropical temperatures. Future work is needed to fully disentangle the contributions of these potential mechanisms.

4. Sensitivity of local precipitation changes to localized absorbing aerosol perturbations

Having investigated the mechanisms governing the sensitivity of global-mean precipitation changes to variations in the geographical location of absorbing aerosol, we now move on to examining the sensitivity of *local* precipitation changes. In Fig. 5 we show the "local" changes in precipitation ($\delta P_{\mathrm{local}}$) in each of the 144 simulations, we define $\delta P_{\mathrm{local}}$ as the fast changes in precipitation averaged over an area containing the 95% of the aerosol perturbation. Our results are not sensitive to this precise definition of $\delta P_{\mathrm{local}}$.

Our results in Fig. 5 demonstrate that the local precipitation response to the radiative effects of absorbing aerosol is generally positive in the deep tropics and switches to negative in the extratropics, in agreement with previous work using both idealized aquaplanet simulations (Dagan et al. 2019) and more realistic AMIP-style simulations (Dagan et al. 2021).

An intuitive way to understand these variations in the local response of precipitation to absorbing aerosol is to consider

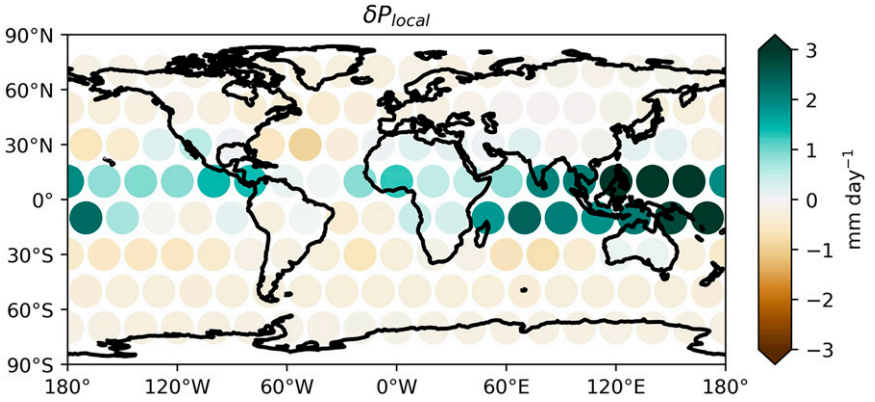

FIG. 5. Map of the local changes in precipitation for each of the 144 aerosol perturbation experiments. Each colored circle represents the results from the simulation imposing an aerosol perturbation in that location. Because of the long integration times (20 years per experiment) and the definition of "local," all of the changes here are significant, and so, in order to keep the plot legible, we have chosen not to add black circles.

the temperature tendency equation for the region covered by the aerosol plume, written as

$$\frac{\partial T}{\partial t} = \frac{\Delta Q_{\text{aero}}}{c_p} + \text{balance terms}, \tag{6}$$

where ΔQ_{aero} represents the (positive) temperature tendency driven by the shortwave absorption from the aerosol plume and c_p is the heat capacity of dry air. In the absence of terms which balance this heating tendency, the temperature in this region would increase without bound. The Planck response helps to balance this shortwave heating tendency, in addition to changes in precipitation and surface fluxes (Williams et al. 2022). Here though we will focus on the role that changes in the atmospheric circulation play in helping to balance this imposed shortwave heating. In the extratropics, linear quasigeostrophic theory (Hoskins and Karoly 1981; Sardeshmukh and Hoskins 1988; Vallis 2017; Williams et al. 2022) predicts that diabatic heating (such as through absorbing aerosol) will tend to result in the formation of a downstream low pressure region and a cyclonic circulation (in the Northern Hemisphere). This is illustrated in Fig. 6, with the low pressure system located over Hudson Bay to the northeast of the aerosol plume. The downstream low helps to balance the heating from the absorbing aerosol by drawing down cold air from higher latitudes. Additionally, this meridional advection of high-latitude air explains the local decrease in precipitation for these extratropical perturbations because the air drawn down by the low pressure system is associated with a lower moisture content and a low relative humidity, both of which inhibit precipitation formation. This decrease in precipitation then also helps to balance the local aerosol heating through a reduction in latent heat release.

In summary, the negative precipitation response to absorbing aerosol in the extratropics can be understood in terms of the atmospheric circulation changes which are required in order to balance the local aerosol heating. This framing can also be used to explain the positive δP_{local} response in the tropics,

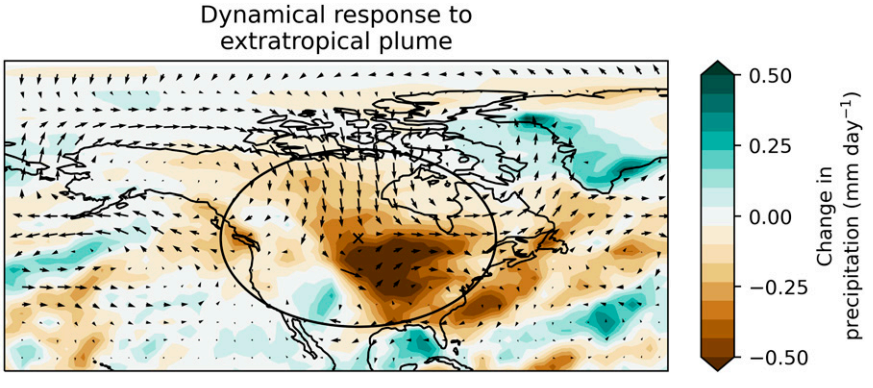

FIG. 6. Map showing the dynamical response of the midlatitude atmospheric circulation to aerosol heating. The black ellipse denotes the area encompassing 95% of the total absorbing aerosol perturbation, the background contours show the change in precipitation compared to the control run and the arrows show the corresponding changes in 850-hPa winds.

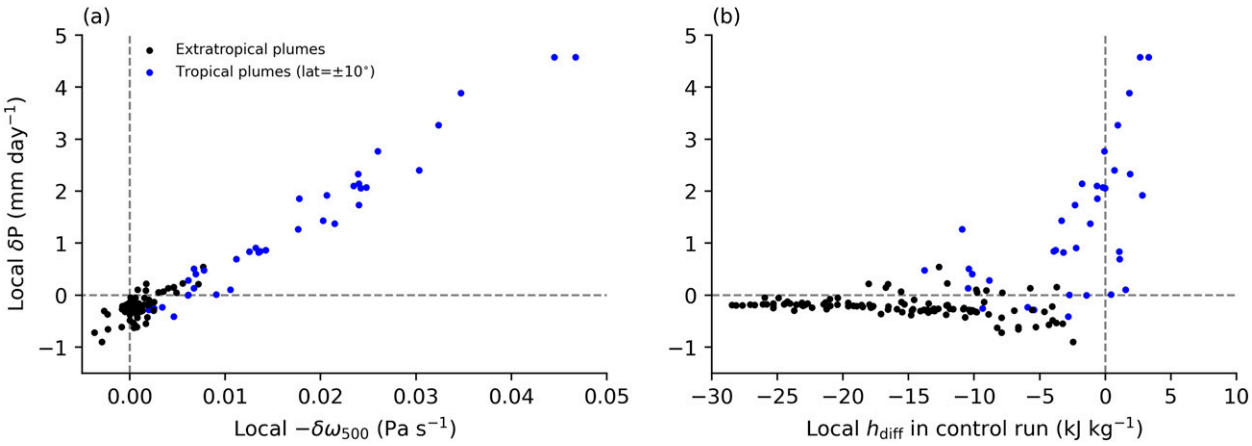

FIG. 7. (a) Scatterplot of local changes in precipitation vs local changes in midtropospheric vertical velocities (ω_{500}), where the $\Delta\omega_{500}$ values have been multiplied by -1, and so, positive values on the x axis indicate increased ascent over the heating region. (b) Scatterplot of local changes in precipitation vs the local h_{diff} over the same region, but in the control run. The h_{diff} coordinate is defined in the main text and acts as a measure of the regions of the tropical atmosphere that are unstable to deep convection.

albeit by a very different set of mechanisms. In the tropics, the weak Coriolis force means that strong gradients of pressure and temperature cannot persist, which is the basis of "weak temperature gradient" (WTG) theories of the tropical atmosphere (e.g., Pierrehumbert 1995; Sobel et al. 2001; Zhang and Fueglistaler 2020; Williams et al. 2023). WTG dictates that diabatic heating anomalies in the tropics (e.g., arising from aerosol absorption) are balanced by adiabatic cooling from increased ascent. This increase in ascent drives an anomalous overturning circulation in the vicinity of the heating, which is associated with low-level moisture convergence and an increase in precipitation (Dagan et al. 2019). Thus, WTG theory qualitatively explains the positive δP_{local} response in the tropics.

So far, we have used a simple framework to explain the contrasting δP_{local} responses between the tropics and the extratropics in terms of the dynamical response of the atmospheric circulation to localized aerosol heating. However, while this framework nicely encapsulates the differing response between the tropics and the extratropics, our results also demonstrate that the longitudinal position of the aerosol is important in determining its local precipitation response, particularly in the tropics. For example, Fig. 5 shows that δP_{local} is much stronger in the western tropical Pacific than in the eastern tropical Pacific and the tropical Atlantic. To understand these varied responses to the longitudinal position of tropical absorbing aerosol, in Fig. 7a we have plotted δP_{local} versus the local change in midtropospheric vertical velocity (ω_{500}) for each of the 144 simulations. Figure 7a demonstrates clearly that stronger local precipitation changes are associated with increased local ascent, which drives a stronger overturning circulation and a larger low-level moisture convergence near the heating region.

While this exercise is a useful sanity check, it does not in and of itself provide us with any predictive power. Indeed, if asked the question, "Which regions do we a priori expect to have a strong local precipitation response to absorbing aerosol?" we would currently be unable to provide an answer. To tackle the questionings of our imagined critic, we follow the work of previous studies (Williams et al. 2009; Williams and Pierrehumbert 2017; Williams et al. 2023) and introduce a simple measure of subcloud buoyancy h_{diff}, which we define as

$$h_{diff} = h_0 - h^*_{500}, \tag{7}$$

where h_0 is the near-surface moist static energy and h^*_{500} is the saturated moist static energy of the free troposphere, again taken at 500 hPa (e.g., Emanuel et al. 1994; Emanuel 2007; Williams et al. 2009; Singh et al. 2017; Williams et al. 2023).[1] The atmosphere is stable against deep convection when h_{diff} is negative, and is unstable to deep convection when h_{diff} is significantly positive. In Fig. 7b we again plot δP_{local} but this time as a function of the local values of h_{diff} over the same region in the control simulation, which shows that the smallest values of δP_{local} occur when the absorbing aerosol is located in regions which are stable to deep convection ($h_{diff} < 0$) and the largest values occur when the aerosol is placed in unstable regions ($h_{diff} > 0$). However, the transition between regions associated with a large δP_{local} and a small δP_{local} does not simply occur at the transition between positive and negative values of h_{diff}, and in fact occurs when h_{diff} is slightly negative. This is because in regions which are weakly stable to deep convection in the control run, the additional heating from the absorbing aerosol causes them to transition to a deeply convective regime with $h_{diff} > 0$ and thus a larger increase in precipitation.

Although it is hard to predict the exact change in h_{diff} which arises due to the absorbing aerosol, we can gain some insight

[1] Similar results are found if we scatter the local change in precipitation against the baseline ω_{500}, but the causality is somewhat confusing here because while ω_{500} is correlated with subcloud buoyancy, it is in fact a result and not a cause of the convection. We also show later on that h_{diff} lets us have more analytical insight into the behavior.

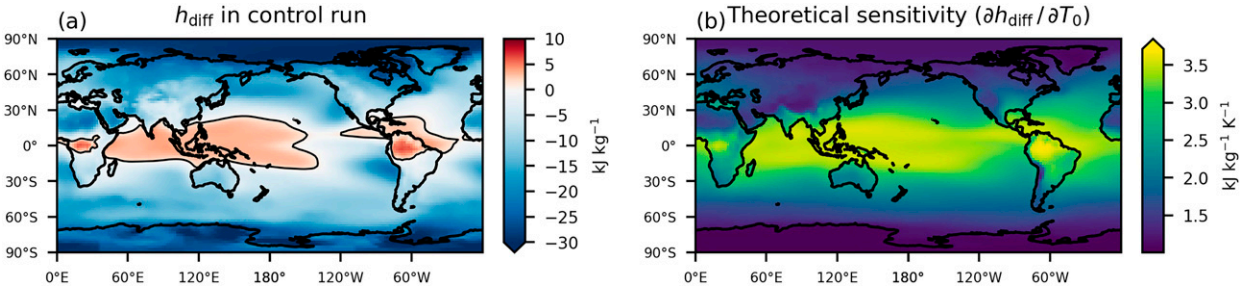

FIG. 8. Map showing the distribution of time-mean (a) h_{diff} in the control run, with the zero contour drawn in black. (b) Also shown is the theoretical sensitivity of h_{diff} to warming calculated using Eq. (6) and using the time-mean air temperature and relative humidity at the lowest model level from the control simulation.

by assuming that the absorption alters h_{diff} primarily by altering h_0 through changes in low-level temperature (δT_0). Noting that $h_0 = c_p T_0 + L_v q_0 + g z_0$, we can write this as

$$\delta h_{diff} = \delta(h_0 - h^*_{500}) \approx \delta h_0 = \delta(c_p T_0 + L_v q_0), \tag{8}$$

where q_0 is the low-level specific humidity, and we have taken the changes at a fixed height. Assuming constant relative humidity (RH), we can also write the $L\delta q_0$ term as

$$\begin{aligned} L_v \delta q_0 &= L_v \, \mathrm{RH}_0 \, \delta[e_s(T_0)] \approx L_v \, \mathrm{RH}_0 \left[\frac{de_s(T_0)}{dT} \delta T_0\right] \\ &= L_v \left[\frac{L_v \mathrm{RH}_0 \, e_s(T_0)}{R_v T_0^2} \delta T_0\right], \end{aligned} \tag{9}$$

where $e_s(T_0)$ is the saturation vapor pressure and we have linearized the saturation vapor pressure around the baseline temperature T_0. Combining this with Eq. (8) we arrive at a simple prediction for δh_{diff} in response to a change in boundary layer temperature:

$$\delta h_{diff} \approx \left[c_p + \frac{\mathrm{RH}_0 L_v^2}{R_v T_0^2} e_s(T_0)\right] \delta T_0. \tag{10}$$

This equation allows us to gain insight into the change in h_{diff} (and thus local precipitation), which may arise due to changes in the boundary layer temperature distribution (δT_0).

In Fig. 8 we plot the baseline distribution of h_{diff} in our control run (Fig. 8a), along with the sensitivity of h_{diff} to warming (e.g., the change which would be associated with a uniform 1-K increase in low-level temperature) (Fig. 8b). The control simulation has positive values of h_{diff} in regions of climatological ascent, as mentioned earlier, with more negative values indicating a strong inversion (e.g., over the Peruvian coast). Note that in our linear framework, the decrease in h_{diff} associated with boundary layer cooling is just the negative of what we have plotted in Fig. 8b.

The theoretical change in h_{diff} associated purely with changes in boundary layer temperature is highest over regions with the highest climatological temperature and humidity (e.g., over the western tropical Pacific or Central and South America). The magnitude of this change in h_{diff} with boundary layer temperature changes is comparable to the magnitude of h_{diff} in the control run over the central Pacific, which again demonstrates that the additional "kick" from the warming effect of absorbing aerosol is able to push regions that were negatively buoyant ($h_{diff} < 0$) in the control run into regions that are positively buoyant ($h_{diff} > 0$) following the perturbation.

Previously we also saw a local decrease in precipitation in response to absorbing aerosol over South America (Fig. 6), and using the h_{diff} framework we can understand this in terms of the surface and boundary layer cooling by the aerosol when placed over land (supplementary Fig. 4). While this region of South America is unstable to deep convection in the control run (i.e., it has $h_{diff} > 0$ in Fig. 8a), the large moisture content of this region also makes it highly susceptible to decreases in h_{diff} from the boundary layer cooling (which is strong over land). This means that for sufficient boundary layer cooling (driven by aerosol scattering and absorption) h_{diff} will eventually become negative, suppressing deep convection and causing a decrease in precipitation locally.

While this framework allows for some basic insights into the response of the tropical atmosphere to absorbing aerosol, it does not account for changes in relative humidity or changes in circulation and moisture advection that would also affect the value of h_{diff} in addition to just the changes which comes from increased low-level temperature. This, along with a more thorough investigation of the response over land and the sensitivity to different land surface properties would be a fruitful avenue for future work.

Relationship with the local atmospheric energy budget

Previous work (Dagan et al. 2019, 2021) has explained the contrasting local precipitation responses to tropical and extratropical absorbing aerosol plumes using a version of the atmospheric energy budget which also accounts for the ability of the atmosphere to converge/diverge dry static energy on local scales, even though this term vanishes on global scales and thus does not appear in Eq. (2). In these studies, they explain that the contrasting response of local precipitation (a local increase in response to tropical aerosol, and a local decrease in response to extratropical aerosol) arises due to the contrasting ability of the atmosphere to diverge excess dry static energy in the two regions. They argue that aerosol heating in the tropics is able to efficiently diverge dry static energy by generating large-scale, thermally driven overturning circulations.

Because of the strong increase in dry static energy with height, even if the magnitude of upper-level divergence is equal and opposite in magnitude to the low-level divergence, such circulations represent a net energy export from the perturbed region. However, as we have shown, this explanation assumes that all regions are susceptible to deep, thermally driven overturning circulations, whereas in the real world zonal asymmetries (such as the Walker circulation) inhibit the formation of such circulations in regions such as the southeastern part of the tropical Pacific (see Fig. 5). Hence, it is important to consider the longitudinal location of the absorbing aerosol when interpreting local precipitation changes, and particularly the aerosol location relative to the existing structure of tropical overturning.

The work of Dagan et al. (2019) also explains the local decrease in response to extratropical aerosol (reproduced in our experiments, Fig. 5) by arguing that the ability of the atmosphere to diverge dry static energy is weaker in the extratropics than the tropics due to variations in the strength of the Coriolis force. They emphasize the process of geostrophic adjustment (Vallis 2017), which is argued to "confine" the aerosol heating to local scales. However, while geostrophic adjustment is a ubiquitous aspect of rotating fluids, it is only able to explain why the atmosphere remains in a state of geostrophic *balance*, and it is not immediately clear that this should result in a localization of the heating anomaly and decrease in precipitation. Here, we have used the argument put forward by Williams et al. (2022) to link the decrease in precipitation in response to extratropical aerosol to the propensity of the atmosphere to balance heating by horizontal advection when presented with strong temperature gradients (as exist in the extratropics).

In summary, our experiments build upon the results of previous work (Dagan et al. 2019, 2021) done with the same ICON model, and we provide an alternative, dynamical perspective to explain these results which is complimentary to the local energetic perspective.

5. Conclusions

Understanding the response of precipitation to anthropogenic changes in atmospheric composition is essential in order to know how to adapt to the changes which will occur over the coming decades. However, understanding the response of precipitation to changes in absorbing aerosol presents a unique challenge due to the highly inhomogeneous spatial pattern of anthropogenic aerosol (which contrasts starkly with well-mixed greenhouse gases such as CO_2), and the complex tropospheric adjustments which occur in response to the diabatic heating from absorbing aerosol. In addition, precipitation changes are commonly separated into "fast" and "slow" components, differentiated by the time scales involved and whether or not they are mediated by SST changes. Previous work has demonstrated that a significant portion of the intermodel spread of precipitation changes in response to black carbon perturbations arises in the fast response (Samset et al. 2016), due to the rapid tropospheric adjustments of clouds and circulation to aerosol heating. However, the complexity of the models used for these studies (where aerosol burden and/or radiative properties are emergent properties rather than prescribed), makes it difficult to understand the mechanisms by which localized absorbing aerosol causes these rapid tropospheric adjustments.

To study the mechanisms by which localized absorbing aerosol in different geographical locations impacts on these rapid adjustments and henceforth to precipitation, we have taken an idealized modeling approach. We have conducted an ensemble of 144 atmosphere-only runs with a state-of-the-art GCM, forced by identical perturbations of aerosol optical depth and radiative properties placed systematically across the whole globe. This idealized approach allows us to explore the basic physics controlling the regional sensitivity of fast precipitation changes to absorbing aerosol.

On global-mean scales, we have found that absorbing aerosol tends to cause a decrease in precipitation in agreement with previous studies (Pendergrass and Hartmann 2012; Samset et al. 2016) and physical reasoning (Pendergrass and Hartmann 2014). However, despite prescribing identical aerosol burdens and radiative properties in each of our experiments, the global-mean precipitation decrease varies by over an order of magnitude between experiments. We explained this by using a global-mean energetic perspective and have linked the spread in global-mean precipitation response to latitudinal variations in incoming solar radiation (Fig. 2), larger surface cooling from the aerosol over land than ocean (Fig. 1c), and large-scale temperature and circulation responses to absorbing aerosol over the western tropical Pacific (Figs. 1b and 3).

The most surprising result from this part of our study is that the global-mean response to absorbing aerosol over the western tropical Pacific is negligible (Fig. 1a). We found that this was associated with stronger changes in global-mean longwave cooling in these experiments, which were driven by changes in global-mean tropospheric temperature. The changes in longwave cooling offset the negative contribution from shortwave absorption, causing a more muted global-mean precipitation response. This result has parallels with the earlier work of (Barsugli and Sardeshmukh 2002), where they found that SST perturbations in the Indo-Pacific led to weaker changes in global-mean precipitation compared to perturbations in the central Pacific. We hypothesize this is due to the enhanced ability of SST anomalies in this region to generate global-mean temperature changes and drive compensating longwave cooling (Barsugli et al. 2006). The first-order importance of circulation adjustments in response to absorbing aerosol over the western tropical Pacific is similar to recent work focusing on the sensitivity of global-mean effective radiative forcing (ERF) to absorbing aerosol (Williams et al. 2022), who showed the circulation adjustments cause this region to be a "hotspot" of ERF from absorbing aerosol.

We have also investigated the changes in "local" precipitation, which generally confirm the findings of previous work which have shown a strong contrast in the local response to absorbing aerosol between the tropics and the extratropics and a weaker response over land than ocean (Dagan et al. 2020, 2021). However, these studies have not systematically explored the sensitivity of these results to the longitudinal position of the aerosol, and our results in Fig. 5 show that the longitudinal position of the aerosol has a large effect on its local precipitation response. In the tropics, we have explained this by introducing a variable (h_{diff}), which uses the boundary

layer temperature and moisture fields to measure the instability of the atmosphere to deep convection. This shows that in regions which are already unstable to deep convection, a boundary layer heating perturbation (such as that provided by absorbing aerosol over the fixed-SST oceans) can cause a strong enhancement of local precipitation. Similar results also hold for marginally stable regions such as the central Pacific, and the decrease in boundary layer temperatures over tropical land also helps to explain the weaker precipitation response in these cases.

We have also provided a dynamical explanation for the local decreases in precipitation in the midlatitudes (Fig. 6) by considering the linear quasigeostrophic response of the atmosphere to diabatic heating. This simple argument, first put forward by Hoskins and Karoly (1981), explains that the tendency of the midlatitude atmosphere is to balance localized heating by horizontal advection of cooler air from the poles via the generation of a downstream low pressure system. This draws down cool air with a low moisture content to the region of the aerosol perturbation, suppressing the precipitation locally over this region. Future work could examine the sensitivity of this result to the vertical location of absorbing aerosol, as this highly local response may break down as the diabatic heating perturbation moves upward and generates a stronger potential vorticity anomaly and potentially a more wavelike response (Lin et al. 2018; Shen and Ming 2018). Repeating our analysis for specific seasons would also be an interesting avenue for future work, particularly when thinking about the local precipitation response.

Finally, as noted throughout the paper, we have only focused on the "fast" precipitation response to absorbing aerosol, and have not included the influence of the aerosol on the SSTs directly (through altering the surface energy balance) or through shifting the large-scale patterns of wind stress or cross-equatorial energy balances (possibly inducing ITCZ shifts; Voigt et al. 2017). In particular, using interactive SSTs may weaken the response of precipitation to absorbing aerosol over the western tropical Pacific, as the SSTs cool in response to the aerosol plume. This would be a fruitful avenue for future work, and it would be useful to include similarly idealized absorbing aerosol perturbations in a hierarchy of slab-ocean and coupled simulations, perhaps focused on only a few regions. Based on our current results, it is sensible to imagine that the local precipitation responses would be weaker if we allowed the aerosol to locally cool the underlying SSTs (e.g., by using a slab ocean) because we see weaker responses of local precipitation to aerosol when the aerosol is located over land (which has an interactive temperature). However, it is not clear what role land–atmosphere interactions play in setting this response, and thus, more targeted experiments are needed to understand these dynamics and link them to future changes in the hydrological cycle.

Acknowledgments. A.I.L. Williams acknowledges funding from the Natural Environment Research Council, Oxford DTP, Award NE/S007474/1. D.W.P. acknowledges funding from NERC Project NE/S005390/1 (ACRUISE) as well as from the European Union's Horizon 2020 research and innovation programme iMIRACLI under Marie Skłodowska-Curie Grant Agreement 860100. P.S. and G.D. were supported by the European Research Council (ERC) project Constraining the Effects of Aerosols on Precipitation (RECAP) under the European Union's Horizon 2020 research and innovation programme with Grant Agreement 724602. P.S. additionally acknowledges funding from the FORCeS and NextGEMs project under the European Union's Horizon 2020 research programme with Grant Agreements 821205 and 101003470, respectively. G.D. also acknowledges funding from the Israeli Science Foundation Grant 1419/21.

The simulations were performed using the ARCHER2 U.K. National Supercomputing Service. Data analysis was performed on JASMIN, the U.K. collaborative data analysis facility, and LOTUS, the associated high performance batch compute cluster.

Data availability statement. Model data from this study are freely available at https://zenodo.org/record/6501508.

REFERENCES

Albrecht, B. A., 1989: Aerosols, cloud microphysics, and fractional cloudiness. *Science*, **245**, 1227–1230, https://doi.org/10.1126/science.245.4923.1227.

Allen, M. R., and W. J. Ingram, 2002: Constraints on future changes in climate and the hydrologic cycle. *Nature*, **419**, 228–232, https://doi.org/10.1038/nature01092.

Ban-Weiss, G. A., L. Cao, G. Bala, and K. Caldeira, 2012: Dependence of climate forcing and response on the altitude of black carbon aerosols. *Climate Dyn.*, **38**, 897–911, https://doi.org/10.1007/s00382-011-1052-y.

Barsugli, J. J., and P. D. Sardeshmukh, 2002: Global atmospheric sensitivity to tropical SST anomalies throughout the Indo-Pacific basin. *J. Climate*, **15**, 3427–3442, https://doi.org/10.1175/1520-0442(2002)015<3427:GASTTS>2.0.CO;2.

——, S.-I. Shin, and P. D. Sardeshmukh, 2006: Sensitivity of global warming to the pattern of tropical ocean warming. *Climate Dyn.*, **27**, 483–492, https://doi.org/10.1007/s00382-006-0143-7.

Brown, H., and Coauthors, 2021: Biomass burning aerosols in most climate models are too absorbing. *Nature Commun.*, **12**, 277, https://doi.org/10.1038/s41467-020-20482-9.

Chemke, R., and L. M. Polvani, 2020: Linking midlatitudes eddy heat flux trends and polar amplification. *npj Climate Atmos. Sci.*, **3**, 8, https://doi.org/10.1038/s41612-020-0111-7.

Crueger, T., and Coauthors, 2018: ICON-A, the atmosphere component of the ICON Earth system model: II. Model evaluation. *J. Adv. Model. Earth Syst.*, **10**, 1638–1662, https://doi.org/10.1029/2017MS001233.

Dagan, G., I. Koren, O. Altaratz, and R. H. Heiblum, 2017: Time-dependent, non-monotonic response of warm convective cloud fields to changes in aerosol loading. *Atmos. Chem. Phys.*, **17**, 7435–7444, https://doi.org/10.5194/acp-17-7435-2017.

——, P. Stier, and D. Watson-Parris, 2019: Contrasting response of precipitation to aerosol perturbation in the tropics and extratropics explained by energy budget considerations. *Geophys. Res. Lett.*, **46**, 7828–7837, https://doi.org/10.1029/2019GL083479.

——, ——, and ——, 2020: Aerosol forcing masks and delays the formation of the North Atlantic warming hole by three decades. *Geophys. Res. Lett.*, **47**, e2020GL090778, https://doi.org/10.1029/2020GL090778.

——, ——, and ——, 2021: An energetic view on the geographical dependence of the fast aerosol radiative effects on precipitation. *J. Geophys. Res. Atmos.*, **126**, e2020JD033045, https://doi.org/10.1029/2020JD033045.

Dong, B., R. T. Sutton, E. J. Highwood, and L. J. Wilcox, 2016: Preferred response of the East Asian summer monsoon to local and non-local anthropogenic sulphur dioxide emissions. *Climate Dyn.*, **46**, 1733–1751, https://doi.org/10.1007/s00382-015-2671-5.

——, L. J. Wilcox, E. J. Highwood, and R. T. Sutton, 2019: Impacts of recent decadal changes in Asian aerosols on the East Asian summer monsoon: Roles of aerosol–radiation and aerosol–cloud interactions. *Climate Dyn.*, **53**, 3235–3256, https://doi.org/10.1007/s00382-019-04698-0.

Emanuel, K., 2007: Quasi-equilibrium dynamics of the tropical atmosphere. *The Global Circulation of the Atmosphere*, Princeton University Press, 186–218.

——, J. D. Neelin, and C. S. Bretherton, 1994: On large-scale circulations in convecting atmospheres. *Quart. J. Roy. Meteor. Soc.*, **120**, 1111–1143, https://doi.org/10.1002/qj.49712051902.

Gates, W. L., 1992: AMIP: The Atmospheric Model Intercomparison Project. *Bull. Amer. Meteor. Soc.*, **73**, 1962–1970, https://doi.org/10.1175/1520-0477(1992)073<1962:ATAMIP>2.0.CO;2.

Giorgetta, M. A., and Coauthors, 2018: ICON-A, the atmosphere component of the ICON Earth system model: I. Model description. *J. Adv. Model. Earth Syst.*, **10**, 1613–1637, https://doi.org/10.1029/2017MS001242.

Herbert, R., P. Stier, and G. Dagan, 2021: Isolating large-scale smoke impacts on cloud and precipitation processes over the Amazon with convection permitting resolution. *J. Geophys. Res. Atmos.*, **126**, e2021JD034615, https://doi.org/10.1029/2021JD034615.

Hoskins, B. J., and D. J. Karoly, 1981: The steady linear response of a spherical atmosphere to thermal and orographic forcing. *J. Atmos. Sci.*, **38**, 1179–1196, https://doi.org/10.1175/1520-0469(1981)038<1179:TSLROA>2.0.CO;2.

——, and T. Ambrizzi, 1993: Rossby wave propagation on a realistic longitudinally varying flow. *J. Atmos. Sci.*, **50**, 1661–1671, https://doi.org/10.1175/1520-0469(1993)050<1661:RWPOAR>2.0.CO;2.

Johnson, B. T., J. M. Haywood, and M. K. Hawcroft, 2019: Are changes in atmospheric circulation important for black carbon aerosol impacts on clouds, precipitation, and radiation? *J. Geophys. Res. Atmos.*, **124**, 7930–7950, https://doi.org/10.1029/2019JD030568.

Kathayat, G., and Coauthors, 2022: Protracted Indian monsoon droughts of the past millennium and their societal impacts. *Proc. Natl. Acad. Sci. USA*, **119**, e2207487119, https://doi.org/10.1073/pnas.2207487119.

Kinne, S., and Coauthors, 2013: MAC-v1: A new global aerosol climatology for climate studies. *J. Adv. Model. Earth Syst.*, **5**, 704–740, https://doi.org/10.1002/jame.20035.

Leuenberger, D., M. Koller, O. Fuhrer, and C. Schär, 2010: A generalization of the SLEVE vertical coordinate. *Mon. Wea. Rev.*, **138**, 3683–3689, https://doi.org/10.1175/2010MWR3307.1.

Levin, Z., and J.-L. Brenguier, 2009: Effects of pollution and biomass aerosols on clouds and precipitation: Observational studies. *Aerosol Pollution Impact on Precipitation: A Scientific Review*, Z. Levin and W. R. Cotton, Eds., Springer, 205–241, https://doi.org/10.1007/978-1-4020-8690-8_6.

Lin, Y., J. Zhang, X. Li, and Y. Deng, 2018: Response of eddy activities to localized diabatic heating in Held–Suarez simulations. *Climate Dyn.*, **51**, 3421–3434, https://doi.org/10.1007/s00382-018-4088-4.

Lohmann, U., and E. Roeckner, 1996: Design and performance of a new cloud microphysics scheme developed for the ECHAM general circulation model. *Climate Dyn.*, **12**, 557–572, https://doi.org/10.1007/BF00207939.

Ming, Y., and V. Ramaswamy, 2009: Nonlinear climate and hydrological responses to aerosol effects. *J. Climate*, **22**, 1329–1339, https://doi.org/10.1175/2008JCLI2362.1.

——, and ——, 2011: A model investigation of aerosol-induced changes in tropical circulation. *J. Climate*, **24**, 5125–5133, https://doi.org/10.1175/2011JCLI4108.1.

Mitchell, J., C. Wilson, and W. Cunnington, 1987: On CO_2 climate sensitivity and model dependence of results. *Quart. J. Roy. Meteor. Soc.*, **113**, 293–322, https://doi.org/10.1002/qj.49711347517.

Muller, C. J., and P. A. O'Gorman, 2011: An energetic perspective on the regional response of precipitation to climate change. *Nat. Climate Change*, **1**, 266–271, https://doi.org/10.1038/nclimate1169.

Myhre, G., and Coauthors, 2017: PDRMIP: A Precipitation Driver and Response Model Intercomparison Project—Protocol and preliminary results. *Bull. Amer. Meteor. Soc.*, **98**, 1185–1198, https://doi.org/10.1175/BAMS-D-16-0019.1.

——, and Coauthors, 2018: Sensible heat has significantly affected the global hydrological cycle over the historical period. *Nat. Commun.*, **9**, 1922, https://doi.org/10.1038/s41467-018-04307-4.

Nordeng, T.-E., 1994: Extended versions of the convective parametrization scheme at ECMWF and their impact on the mean and transient activity of the model in the tropics. ECMWF Tech. Memo. 206, 41 pp., https://www.ecmwf.int/en/elibrary/75843-extended-versions-convective-parametrization-scheme-ecmwf-and-their-impact-mean.

Pendergrass, A. G., and D. L. Hartmann, 2012: Global-mean precipitation and black carbon in AR4 simulations. *Geophys. Res. Lett.*, **39**, L01703, https://doi.org/10.1029/2011GL050067.

——, and ——, 2014: The atmospheric energy constraint on global-mean precipitation change. *J. Climate*, **27**, 757–768, https://doi.org/10.1175/JCLI-D-13-00163.1.

Persad, G. G., 2023: The dependence of aerosols' global and local precipitation impacts on the emitting region. *Atmos. Chem. Phys.*, **23**, 3435–3452, https://doi.org/10.5194/acp-23-3435-2023.

——, and K. Caldeira, 2018: Divergent global-scale temperature effects from identical aerosols emitted in different regions. *Nat. Commun.*, **9**, 3289, https://doi.org/10.1038/s41467-018-05838-6.

——, Y. Ming, and V. Ramaswamy, 2012: Tropical tropospheric-only responses to absorbing aerosols. *J. Climate*, **25**, 2471–2480, https://doi.org/10.1175/JCLI-D-11-00122.1.

Pierrehumbert, R. T., 1995: Thermostats, radiator fins, and the local runaway greenhouse. *J. Atmos. Sci.*, **52**, 1784–1806, https://doi.org/10.1175/1520-0469(1995)052<1784:TRFATL>2.0.CO;2.

Pincus, R., and B. Stevens, 2013: Paths to accuracy for radiation parameterizations in atmospheric models. *J. Adv. Model. Earth Syst.*, **5**, 225–233, https://doi.org/10.1002/jame.20027.

Ramanathan, V., P. J. Crutzen, J. T. Kiehl, and D. Rosenfeld, 2001: Aerosols, climate, and the hydrological cycle. *Science*, **294**, 2119–2124, https://doi.org/10.1126/science.1064034.

Samset, B. H., and Coauthors, 2016: Fast and slow precipitation responses to individual climate forcers: A PDRMIP multimodel study. *Geophys. Res. Lett.*, **43**, 2782–2791, https://doi.org/10.1002/2016GL068064.

Sardeshmukh, P. D., and B. J. Hoskins, 1988: The generation of global rotational flow by steady idealized tropical divergence. *J. Atmos. Sci.*, **45**, 1228–1251, https://doi.org/10.1175/1520-0469(1988)045<1228:TGOGRF>2.0.CO;2.

Seifert, A., T. Heus, R. Pincus, and B. Stevens, 2015: Large-eddy simulation of the transient and near-equilibrium behavior of precipitating shallow convection. *J. Adv. Model. Earth Syst.*, **7**, 1918–1937, https://doi.org/10.1002/2015MS000489.

Shen, Z., and Y. Ming, 2018: The influence of aerosol absorption on the extratropical circulation. *J. Climate*, **31**, 5961–5975, https://doi.org/10.1175/JCLI-D-17-0839.1.

Singh, M. S., Z. Kuang, and Y. Tian, 2017: Eddy influences on the strength of the Hadley circulation: Dynamic and thermodynamic perspectives. *J. Atmos. Sci.*, **74**, 467–486, https://doi.org/10.1175/JAS-D-16-0238.1.

Sobel, A. H., J. Nilsson, and L. M. Polvani, 2001: The weak temperature gradient approximation and balanced tropical moisture waves. *J. Atmos. Sci.*, **58**, 3650–3665, https://doi.org/10.1175/1520-0469(2001)058<3650:TWTGAA>2.0.CO;2.

Stevens, B., and G. Feingold, 2009: Untangling aerosol effects on clouds and precipitation in a buffered system. *Nature*, **461**, 607–613, https://doi.org/10.1038/nature08281.

——, and Coauthors, 2013: Atmospheric component of the MPI-M Earth System Model: ECHAM6. *J. Adv. Model. Earth Syst.*, **5**, 146–172, https://doi.org/10.1002/jame.20015.

——, S. Fiedler, S. Kinne, K. Peters, S. Rast, J. Müsse, S. J. Smith, and T. Mauritsen, 2017: MACv2-SP: A parameterization of anthropogenic aerosol optical properties and an associated Twomey effect for use in CMIP6. *Geosci. Model Dev.*, **10**, 433–452, https://doi.org/10.5194/gmd-10-433-2017.

Stier, P., J. H. Seinfeld, S. Kinne, and O. Boucher, 2007: Aerosol absorption and radiative forcing. *Atmos. Chem. Phys.*, **7**, 5237–5261, https://doi.org/10.5194/acp-7-5237-2007.

Stjern, C. W., and Coauthors, 2017: Rapid adjustments cause weak surface temperature response to increased black carbon concentrations. *J. Geophys. Res. Atmos.*, **122**, 11 462–11 481, https://doi.org/10.1002/2017JD027326.

——, and Coauthors, 2023: The time scales of climate responses to carbon dioxide and aerosols. *J. Climate*, **36**, 3537–3551, https://doi.org/10.1175/JCLI-D-22-0513.1.

Sundqvist, H., E. Berge, and J. Kristjánsson, 1989: Condensation and cloud parameterization studies with a mesoscale numerical weather prediction model. *Mon. Wea. Rev.*, **117**, 1641–1657, https://doi.org/10.1175/1520-0493(1989)117<1641:CACPSW>2.0.CO;2.

Tian, F., B. Dong, J. Robson, and R. Sutton, 2018: Forced decadal changes in the East Asian summer monsoon: The roles of greenhouse gases and anthropogenic aerosols. *Climate Dyn.*, **51**, 3699–3715, https://doi.org/10.1007/s00382-018-4105-7.

Tiedtke, M., 1989: A comprehensive mass flux scheme for cumulus parameterization in large-scale models. *Mon. Wea. Rev.*, **117**, 1779–1800, https://doi.org/10.1175/1520-0493(1989)117<1779:ACMFSF>2.0.CO;2.

Vallis, G. K., 2017: *Atmospheric and Oceanic Fluid Dynamics: Fundamentals and Large-Scale Circulation.* 2nd ed. Cambridge University Press, 946 pp., https://doi.org/10.1017/9781107588417.

Voigt, A., and Coauthors, 2017: Fast and slow shifts of the zonal-mean intertropical convergence zone in response to an idealized anthropogenic aerosol. *J. Adv. Model. Earth Syst.*, **9**, 870–892, https://doi.org/10.1002/2016MS000902.

Wang, C., 2004: A modeling study on the climate impacts of black carbon aerosols. *J. Geophys. Res.*, **109**, D03106, https://doi.org/10.1029/2003JD004084.

——, 2007: Impact of direct radiative forcing of black carbon aerosols on tropical convective precipitation. *Geophys. Res. Lett.*, **34**, L05709, https://doi.org/10.1029/2006GL028416.

——, 2015: Anthropogenic aerosols and the distribution of past large-scale precipitation change. *Geophys. Res. Lett.*, **42**, 10 876–10 884, https://doi.org/10.1002/2015GL066416.

Watanabe, M., Y. Kamae, H. Shiogama, A. M. DeAngelis, and K. Suzuki, 2018: Low clouds link equilibrium climate sensitivity to hydrological sensitivity. *Nat. Climate Change*, **8**, 901–906, https://doi.org/10.1038/s41558-018-0272-0.

Westervelt, D. M., and Coauthors, 2018: Connecting regional aerosol emissions reductions to local and remote precipitation responses. *Atmos. Chem. Phys.*, **18**, 12 461–12 475, https://doi.org/10.5194/acp-18-12461-2018.

Williams, A. I., P. Stier, G. Dagan, and D. Watson-Parris, 2022: Strong control of effective radiative forcing by the spatial pattern of absorbing aerosol. *Nat. Climate Change*, **12**, 735–742, https://doi.org/10.1038/s41558-022-01415-4.

——, N. Jeevanjee, and J. Bloch-Johnson, 2023: Circus tents, convective thresholds and the non-linear climate response to tropical SSTs. *Geophys. Res. Lett.*, **50**, e2022GL101499, https://doi.org/10.1029/2022GL101499.

Williams, I. N., and R. T. Pierrehumbert, 2017: Observational evidence against strongly stabilizing tropical cloud feedbacks. *Geophys. Res. Lett.*, **44**, 1503–1510, https://doi.org/10.1002/2016GL072202.

——, ——, and M. Huber, 2009: Global warming, convective threshold and false thermostats. *Geophys. Res. Lett.*, **36**, L21805, https://doi.org/10.1029/2009GL039849.

Xie, X., and Coauthors, 2020: Distinct responses of Asian summer monsoon to black carbon aerosols and greenhouse gases. *Atmos. Chem. Phys.*, **20**, 11 823–11 839, https://doi.org/10.5194/acp-20-11823-2020.

Zhang, S., P. Stier, and D. Watson-Parris, 2021: On the contribution of fast and slow responses to precipitation changes caused by aerosol perturbations. *Atmos. Chem. Phys.*, **21**, 10 179–10 197, https://doi.org/10.5194/acp-21-10179-2021.

Zhang, Y., and S. Fueglistaler, 2020: How tropical convection couples high moist static energy over land and ocean. *Geophys. Res. Lett.*, **47**, e2019GL086387, https://doi.org/10.1029/2019GL086387.